inter·noise 2021
1–5 August | Washington, DC

Predicting the diffuse vibration transmission across finite junctions between thick plates

Wannes Stalmans[1], Cédric Van hoorickx[2] and Edwin Reynders [3]
KU Leuven
Kasteelpark Arenberg 40, 3001 Leuven, Belgium

ABSTRACT

Predicting the sound insulation of an engineering system is a complex problem since both direct and flanking transmission can largely influence the sound insulation of the system. When conventionally analyzing flanking transmission, walls and floors are modelled as thin homogeneous plates and the junction is assumed to be of infinite extent. For thick walls or floors and junctions of finite length, it is not immediately obvious how this approach can be adapted. A new approach based on diffuse field reciprocity is proposed to overcome the limitations of the conventional approach. The diffuse field reciprocity relationship can be used to calculate the total energy in a vibrating subsystem based on the direct field dynamic stiffness matrix of the subsystem, i.e., the dynamic stiffness of the equivalent infinite subsystem as observed at the junction. The direct field dynamic stiffness matrix of a thin, isotropic, semi-infinite plate can be analytically derived. For thick or more complex walls or floors the direct field dynamic stiffness can be calculated using finite elements and perfectly matched layers. Using this new approach for calculating vibration transmission across junctions, practical design curves are determined.

1. INTRODUCTION

Effective protection from noise disturbance can be achieved by ensuring sufficient sound insulation in buildings. Unfortunately, this is a complex technical problem, since design details and multiple transmission paths can strongly influence the sound insulation [1]. Both the direct transmission through the element as well as the flanking transmission can impact the overall sound insulation between two rooms.

When conventionally analyzing flanking transmission, a diffuse field is assumed in walls and floors, which are modelled as plates. Junctions connecting the walls and floors are assumed to be infinite and the transmission of vibration across the junction is calculated by integrating the plane-wave transmission over all possible angles of incidence. Examples of this approach for homogeneous plate systems can be found in [2–4]. It is not immediately obvious how this conventional approach can be adapted to take the finite junction length into account, or to model more complex systems.

[1]wannes.stalmans@kuleuven.be

[2]cedric.vanhoorickx@kuleuven.be

[3]edwin.reynders@kuleuven.be

To address these limitations, an approach based on diffuse field reciprocity is proposed here. The diffuse field reciprocity relationship relates the blocked reverberant forces in a a vibrating subsystem at the junction to the direct field dynamic stiffness [5], i.e., the dynamic stiffness of the equivalent unbounded subsystem as observed at the finite junction. The direct field dynamic stiffness matrices in the wavenumber domain can be analytically derived for thin, isotropic, semi-infinite plates, as described by Langley and Heron [4]. Since the assumption of thin plates is only valid at low frequencies, another method is proposed here to determine the direct field dynamic stiffness using a combination of finite elements and perfectly matched layers. With this method a combination of 2.5D finite elements and perfectly matched layers is used to model a semi-infinite plate. The 2.5D finite elements allow modelling the 3D plate with a 2D mesh, taking into account that the plate is infinite along the junction. This is combined with a perfectly matched layer which absorbs outgoing waves to model the semi-infinite plate in the direction perpendicular to the junction.

In the presented work, both methods are used to calculate direct field dynamic stiffness along the finite junction in the spatial domain by introducing a correction for baffled boundary conditions. The transmission losses found with the new approach proposed here are compared to the regression curves found in ISO 12354-1 [6], Annex E.4. These expressions were found using simulations with the finite elements method (FEM), the spectral finite element method (SFEM) and wave theory [7].

2. METHODOLOGY

2.1. Determination of transmission coefficient

A finite junction is considered with a junction length L and N plates connected to the junction, as shown in Figure 1. The problem addressed in this paper is to calculate the transmission coefficient, which is defined as the ratio of the power transmitted through the junction from plate j to plate l to the power that is incident on the junction [1].

$$\tau_{jl} = \frac{W_{jl}}{W_{\mathrm{inc},j}} \tag{1}$$

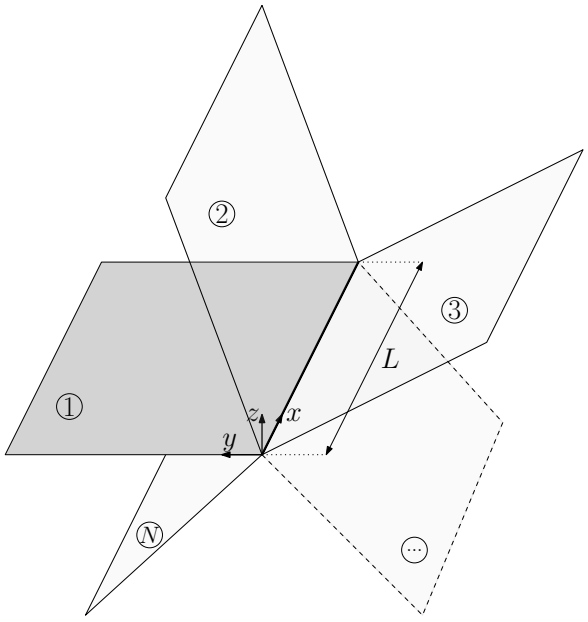

Figure 1: Number of plates connected to a finite junction with length L.

When conventionally analyzing flanking transmission, the transmission coefficient $\tau_{jl}(\phi)$ from subsystem j to subsystem l is calculated for multiple incident wave angles ϕ and then integrated to calculate the mean diffuse field transmission coefficient $\hat{\tau}_{jl}$.

$$\hat{\tau}_{jl} = \frac{1}{2} \int_{-\frac{\pi}{2}}^{\frac{\pi}{2}} \tau_{jl}(\phi) \cos(\phi) \, \mathrm{d}\phi \tag{2}$$

The transmission coefficient $\tau_{jl}(\phi)$ for an incident wave with heading ϕ can be calculated using a dynamic stiffness approach, as done by Langley and Heron [4]. In that work, the direct field dynamic stiffness matrices of a thin, isotropic, elastic plate are derived in the wavenumber domain using thin plate theory.

Due to the limitations of the conventional approach, a new approach is presented here, in which the diffuse field transmission coefficient $\hat{\tau}_{jl}$ is calculated via the coupling loss factor $\hat{\eta}_{jl}$. The relation between these two is given by the following equation [8]

$$\hat{\tau}_{jl} = \frac{\omega \pi S_j}{c_{\mathrm{g},j} L} \hat{\eta}_{jl} \tag{3}$$

in which S_j is the surface of plate j, $c_{\mathrm{g},j}$ is the group velocity of the considered wavetype in plate j and $\hat{\tau}_{jl}$ is the diffuse field transmission coefficient between the considered wave types of subsystems j and l.

The coupling loss factor can be determined with the following formula, which is derived using diffuse field reciprocity [5]

$$\hat{\eta}_{jl} = \frac{2 \sum_{r,s} \mathrm{Im}\left(\mathbf{D}^{(l)}_{\mathrm{dir},rs}\right) \left(\mathbf{D}^{-1}_{\mathrm{tot}} \mathrm{Im}\left(\mathbf{D}^{(j)}_{\mathrm{dir}}\right) \mathbf{D}^{-\mathrm{H}}_{\mathrm{tot}}\right)_{rs}}{\omega \pi n_j} \tag{4}$$

in which $\mathbf{D}^{(j)}_{\mathrm{dir}}$ is the direct field dynamic stiffness matrix of subsystem j, $\mathbf{D}_{\mathrm{tot}} = \sum_{j=1}^{N} \mathbf{D}^{(j)}_{\mathrm{dir}}$ and n_j is the modal density of the considered subsystem of plate j:

$$n_j = \frac{S_j k_j}{2\pi c_{\mathrm{g},j}} \tag{5}$$

in which k_j is the wavenumber of the considered wavetype in plate j. Combining equations (3), (4) and (5), gives the expression below for calculating the diffuse field transmission coefficient,

$$\hat{\tau}_{jl} = \frac{4\pi}{L k_j} \sum_{r,s} \mathrm{Im}\left(\mathbf{D}^{(l)}_{\mathrm{dir},rs}\right) \left(\mathbf{D}^{-1}_{\mathrm{tot}} \mathrm{Im}\left(\mathbf{D}^{(j)}_{\mathrm{dir}}\right) \mathbf{D}^{-\mathrm{H}}_{\mathrm{tot}}\right)_{rs} \tag{6}$$

Equation (6) shows that the diffuse field transmission coefficient for the transmission of bending waves depends on the junction length, the bending wavenumber of the excited plate and the direct field dynamic stiffness matrices of all plates that are connected to the junction. The direct field dynamic stiffness matrix is the dynamic stiffness of the equivalent unbounded subsystem as observed at the finite junction of a considered subsystem, it can be determined in multiple ways. Two possible methods will be discussed, where the first uses thin plate theory to analytically derive the direct field dynamic stiffness matrix of a thin, isotropic, semi-infinite plate in the wavenumber domain. A second method uses a combination of 2.5D finite elements and perfectly matched layers to determine the direct field dynamic stiffness matrix in the wavenumber domain.

2.2. Derivation using thin plate theory

The direct field dynamic stiffness matrix of a thin, isotropic, elastic semi-infinite plate in the wavenumber domain in the local coordinate system of the plate can be calculated as follows. The transformation from the wavenumber domain to the spatial domain will be discussed in section 2.4. Since the in-plane (IP) and out-of-plane (OOP) behavior of the plate are decoupled, the direct field dynamic stiffness matrix is a block diagonal matrix [4]

$$\mathbf{D}_{\text{dir}}^{(j)'}(k_x) = \begin{bmatrix} \mathbf{D}_{\text{dir,IP}}^{(j)'}(k_x) & \mathbf{0} \\ \mathbf{0} & \mathbf{D}_{\text{dir,OOP}}^{(j)'}(k_x) \end{bmatrix} \tag{7}$$

$$\mathbf{D}_{\text{dir,IP}}^{(j)'}(k_x) = \frac{E_j t_j}{k_x^2 - \mu_{\text{S}}\mu_{\text{L}}} \begin{bmatrix} -\frac{\left(\mu_{\text{S}}^2 - k_x^2\right)\mu_{\text{L}}}{2\left(1+\nu_j\right)} & \frac{-\text{i}\left(\mu_{\text{L}}^2 - \nu_j k_x^2\right)k_x}{1-\nu_j^2} + \frac{\text{i}\mu_{\text{S}}\mu_{\text{L}}k_x}{1+\nu_j} \\ \frac{\text{i}\left(\mu_{\text{L}}^2 - \nu_j k_x^2\right)k_x}{1-\nu_j^2} - \frac{\text{i}\mu_{\text{S}}\mu_{\text{L}}k_x}{1+\nu_j} & \frac{\left(\nu_j k_x^2 - \mu_{\text{L}}^2\right)\mu_{\text{s}}}{1-\nu_j^2} + \frac{k_x^2\mu_{\text{S}}}{1+\nu_j} \end{bmatrix} \tag{8}$$

$$\mathbf{D}_{\text{dir,OOP}}^{(j)'}(k_x) = E_j t_j \begin{bmatrix} \frac{\mu_{\text{B1}}^3\mu_{\text{B2}} - \mu_{\text{B2}}^3\mu_{\text{B1}}}{12\left(1-\nu_j^2\right)\left(\mu_{\text{B1}} - \mu_{\text{B2}}\right)} & \frac{\mu_{\text{B2}}^3 - \mu_{\text{B1}}^3 + \left(1-\nu_j\right)\left(\mu_{\text{B1}} - \mu_{\text{B2}}\right)k_x^2}{12\left(1-\nu_j^2\right)\left(\mu_{\text{B1}} - \mu_{\text{B2}}\right)} \\ \frac{\mu_{\text{B2}}^3 - \mu_{\text{B1}}^3 + \left(1-\nu_j\right)\left(\mu_{\text{B1}} - \mu_{\text{B2}}\right)k_x^2}{12\left(1-\nu_j^2\right)\left(\mu_{\text{B1}} - \mu_{\text{B2}}\right)} & \frac{\mu_{\text{B1}}^2 - \mu_{\text{B2}}^2}{12\left(1-\nu_j^2\right)\left(\mu_{\text{B1}} - \mu_{\text{B2}}\right)} \end{bmatrix} \tag{9}$$

where k_x is the wavenumber in the x-direction, E_j and ν_j are the Young's modulus and the Poisson's ratio of plate j, respectively, and

$$\mu_{\text{L}} = -\sqrt{k_x^2 - k_{\text{L}}^2} \qquad \mu_{\text{S}} = -\sqrt{k_x^2 - k_{\text{S}}^2} \tag{10}$$

$$\mu_{\text{B1}} = -\sqrt{k_x^2 + k_{\text{B}}^2} \qquad \mu_{\text{B2}} = -\sqrt{k_x^2 - k_{\text{B}}^2} \tag{11}$$

The longitudinal, transverse shear-wave, and bending wavenumbers can be calculated using respectively

$$k_{\text{L}} = 2\pi f \sqrt{\frac{\rho_j\left(1-\nu_j^2\right)}{E_j}}, \tag{12}$$

$$k_{\text{S}} = 2\pi f \sqrt{\frac{2\rho_j\left(1+\nu_j\right)}{E_1}}, \tag{13}$$

$$k_{\text{B}} = \left(\frac{12\left(2\pi f\right)^2\rho_j\left(1-\nu_j^2\right)}{E_j t_j^2}\right)^{\frac{1}{4}}. \tag{14}$$

2.3. 2.5D finite elements with perfectly matched layers

The direct field dynamic stiffness of a plate can also be calculated using a combination of finite elements and perfectly matched layers, as shown in figure 2. Since the semi-infinite plate is infinite along the junction in the x-direction, a 2.5D approach can be applied to model the semi-infinite plate in the x-direction. The x-coordinate is transformed to the wavenumber k_x with a Fourier transform to allow representing the 3D response of the structure and the radiated wavefield on a two-dimensional mesh [9]. Since the semi-infinite plate is also infinite in the positive y-direction, the 2.5D finite elements are combined with a perfectly matched layer. The perfectly matched layer surrounding the finite element model absorbs the wave propagating outwards from the bounded domain, thus simulating an unbounded subsystem [10]. A schematic representation of the model can be seen in figure 2. In the domain where $0 \leq y \leq L_y$, quadratic 8-node elements are used which are coupled to the quadratic 8-node elements perfectly matched layer elements used in the domain $L_y \leq y \leq L_y + L_{\text{PML}}$.

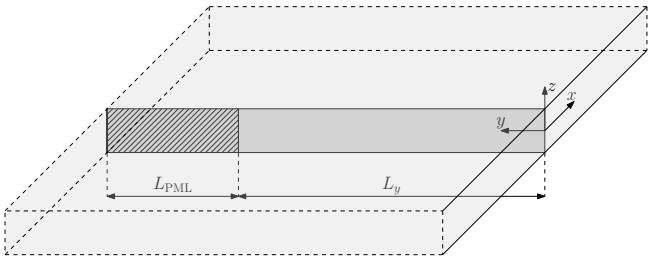

Figure 2: 2.5D model of a semi-infinite plate.

2.4. Transformation to the spatial domain of the direct field dynamic stiffness matrix

To take into account the finite length of the junction, the direct field dynamic stiffness matrices of the plates connected to the junction are transformed to the spatial domain. A method using a correction for baffled boundary conditions is introduced to calculate the direct field dynamic stiffness matrix of a semi-infinite plate in the spatial domain. The correction for baffled boundary conditions consists of first expressing the displacements of the junction as a linear combination of a set of shape functions

$$\mathbf{q} = \begin{bmatrix} u(x) \\ v(x) \\ w(x) \\ \theta(x) \end{bmatrix} = \sum_s q_s \phi_s(x) \tag{15}$$

in which ϕ_s is a vector with four components (translations in x-, y-, and z-direction and a rotation about the x-axis). The shape functions are constructed as follows

$$\begin{bmatrix} \varphi_1 \\ 0 \\ 0 \\ 0 \end{bmatrix}, \begin{bmatrix} 0 \\ \varphi_1 \\ 0 \\ 0 \end{bmatrix}, \begin{bmatrix} 0 \\ 0 \\ \varphi_1 \\ 0 \end{bmatrix}, \begin{bmatrix} 0 \\ 0 \\ 0 \\ \varphi_1 \end{bmatrix}, \begin{bmatrix} \varphi_2 \\ 0 \\ 0 \\ 0 \end{bmatrix}, \begin{bmatrix} 0 \\ \varphi_2 \\ 0 \\ 0 \end{bmatrix}, \dots \tag{16}$$

in which φ_n is the nth sine function (sine functions are used since baffled boundary conditions are considered outside the junction):

$$\varphi_n(x) = \begin{cases} 0 & \text{if} \quad x < 0 \\ \sin\left(\frac{n\pi x}{L}\right) & \text{if} \quad 0 \le x \le L \\ 0 & \text{if} \quad x > L. \end{cases} \tag{17}$$

The shape functions φ_n are transformed from the spatial domain to the wavenumber domain. Due to the baffled boundary conditions the integration is limited from 0 to L.

$$\begin{aligned} \Phi_n(k_x) &= \int_0^L \varphi_n(x)\, \mathrm{e}^{-\mathrm{i}k_x x} \mathrm{d}x \\ &= \frac{\mathrm{e}^{\mathrm{i}\left(k_x - \frac{n\pi}{L}\right)L} - 1}{2\left(k_x - \frac{n\pi}{L}\right)} + \frac{1 - \mathrm{e}^{\mathrm{i}\left(k_x + \frac{n\pi}{L}\right)L}}{2\left(k_x + \frac{n\pi}{L}\right)} \end{aligned} \tag{18}$$

The corrected direct field dynamic stiffness matrix can now be calculated using [11]

$$\mathrm{D}^{(j)}_{\mathrm{dir},nm} = \frac{1}{2\pi} \int_{-\infty}^{\infty} \mathbf{\Phi}^{\mathrm{H}}_n(k_x)\, \mathbf{D}^{(j)}_{\mathrm{dir}}(k_x)\, \mathbf{\Phi}_m(k_x)\, \mathrm{d}k_x \tag{19}$$

in which $\mathbf{\Phi}_n$ is a vector with four component consisting of the shape functions in the wavenumber domain, $\mathbf{D}_{\text{dir}}^{(j)}$ is defined in the global coordinate system and H is the Hermitian transpose. The direct field dynamic stiffness matrix $\mathbf{D}_{\text{dir}}^{(j)'}$ is defined in the local coordinate system of plate j and has to be transformed to the global coordinate system [4]

$$\mathbf{D}_{\text{dir}}^{(j)} = \mathbf{R}_j \mathbf{D}_{\text{dir}}^{(j)'} \mathbf{R}_j^{\text{T}} \tag{20}$$

where the transformation matrix $\mathbf{R}_j$ transforms the direct field dynamic stiffness matrix from the local coordinate system to the global coordinate system.

Numerical integration is used for evaluating the integral in equation (19). The wavenumbers are sampled linearly; the number of samples and the upper limit wavenumber value are determined based on the convergence of the solution of the transmission coefficients.

3. CASE STUDY: L-JUNCTION

The proposed approach will now be applied to an L-junction consisting of two perpendicular plates, as shown in figure 3.

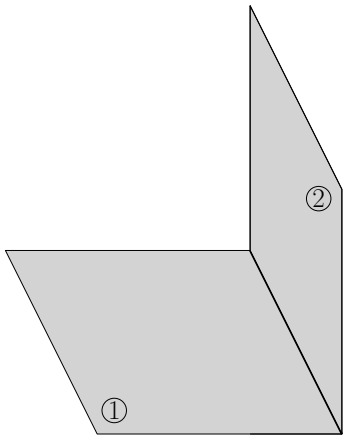

Figure 3: L-junction.

The materials used for the plates in the simulations can be found in table 1. Materials 1 and 2 are used for plate 1 while materials 1 to 6 are used for plate 2. The junction length is varied from 2 m to 8 m in steps of 1 m.

Table 1: Material properties

Material	Internal loss factor η_{int} [-]	Density ρ [kg/m^3]	Quasi-longitudinal wavespeed c_{L} [m/s]	Poisson ratio ν [-]
1: Concrete	0.005	2200	3800	0.2
2: Brick	0.01	1750	2700	0.2
3: Aerated concrete	0.0125	800	1900	0.2
4: Lightweight aggregate	0.01	1400	1400	0.2
5: Dense aggregate	0.01	2000	3200	0.2
6: Calcium-silicate	0.01	1800	2500	0.2

The thickness of plate 1 is varied from 0.05 m to 0.4 m. To determine the thickness of the second perpendicular plate, the ratio of characteristic moment impedances is varied from 0.01 to 300. This sometimes results in an unrealistic thickness for plate 2. Results for thicknesses of plate 2 larger than 0.5 m are filtered out. The ratio of characteristic moment impedances $\frac{\psi}{\chi}$ is used as the independent variable when plotting results as proposed by Cremer and Heckl [3]. This ratio is given by

$$\frac{\psi}{\chi} = \sqrt[4]{\frac{m'_{\perp j} B^3_{\perp j}}{m'_j B^3_j}} \tag{21}$$

where m'_j is the mass per unit area of element j, $m'_{\perp j}$ is the mass per unit area of the element perpendicular to element j, B_j is the bending stiffness of element j and $B_{\perp j}$ is the bending stiffness of the element perpendicular to element j.

Using a set of junctions with the properties described above, the diffuse bending wave transmission coefficient is calculated in one-third octave band centre frequencies from 50 Hz to 3150 Hz with the method described in section 2. Following ISO 12354-1, The low-frequency range is defined as the one-third octave bands from 50 Hz to 200 Hz, the mid-frequency range from 250 Hz to 1000 Hz and the high-frequency range from 1250 Hz to 3150 Hz. Results show that both methods for determining the direct field dynamic stiffness result in the same transmission coefficient values in the low frequency range. The analytical expressions for the direct field dynamic stiffness are thus used in the low-frequency range since these are more computationally efficient. In the mid- and high-frequency range the direct field dynamic stiffness is determined using 2.5D finite elements combined with perfectly matched layers. A single value for the transmission coefficient is found by calculating the arithmetic average in the considered frequency range.

Figure 4 shows the transmission losses found in the low-frequency range with the new approach, together with the regression curves from ISO 12354-1 [6]. Here it can be seen that the new approach results in a prediction for the transmission loss that is generally higher than the regression curve from the international standard, which was determined using a combination of finite elements methods (FEM), spectral finite element methods (SFEM) and wave theory. Wave theory assumes an infinite junction, which results in lower transmission losses compared to finite elements. This could also be seen in the work of Hopkins et al. [7] where junctions length of 4, 5, and 6 m were used, while the results shown here use junctions lengths from 2 to 8 m, adding to the higher transmission losses seen here. Figure 4 shows that the junction length has an influence on the transmission loss in the low frequency range. This is due to the bending wavelengths in the plates being large compared to the length of the junction in this frequency range, since in the low frequency range there mainly is transmission of bending waves. Since the influence of the length of the junction can be seen in figure 4, regression curves can be determined where the length of the junction is considered. The independent variable is PC:

$$\mathrm{PC} = \log\left(\frac{\psi}{\chi}\right) \tag{22}$$

where $\frac{\psi}{\chi}$ is the ratio of characteristic moment impedances (see formula 21). Cubic polynomials are used ($A \cdot \mathrm{PC}^3 + B \cdot \mathrm{PC}^2 + C \cdot \mathrm{PC} + D$) to fit regression curves through the data for the transmission losses per junction length. The parameters of the regression curves can be found in table 2, together with the coefficient of determination R^2 of the regression curve.

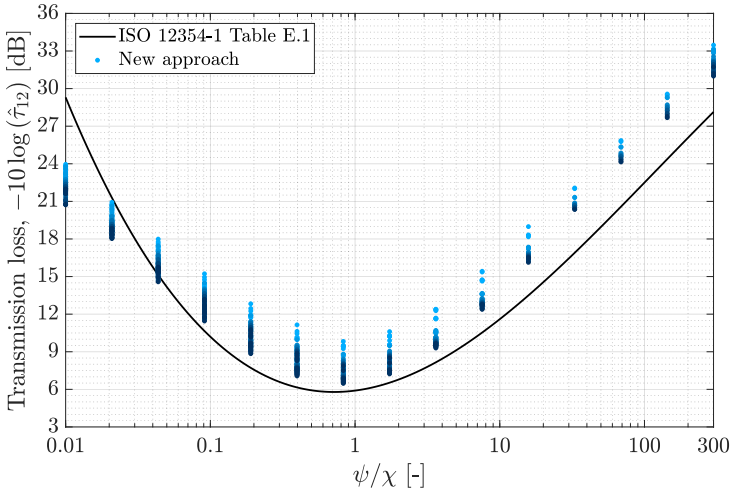

Figure 4: Results using the new approach in low-frequency range (50-200 Hz) together with the regression curve from ISO 12354-1. Lightblue dots correspond to a junction length of 2 m and darkblue to a junction length of 8 m. The colors used for plotting results of intermediate junction lengths are interpolated between light- and darkblue.

Table 2: Regression curve parameters and coefficient of determination R^2 in the low-frequency range.

Junction length	A	B	C	D	R^2
2 m	-0.13	3.80	1.13	10.39	0.975
3 m	-0.11	4.00	1.01	9.09	0.979
4 m	-0.10	3.97	0.94	8.68	0.975
5 m	-0.10	3.96	0.94	8.48	0.974
6 m	-0.10	3.94	0.95	8.34	0.973
7 m	-0.10	3.91	0.96	8.23	0.972
8 m	-0.10	3.88	0.97	8.15	0.971

In table 2 it can be seen that the first three parameters (A, B and C) only vary slightly for the different junction lengths while D does vary clearly as a function of the junction length. Due to this, a single regression curve is proposed which is raised or lowered depending on the junction length:

$$\mathrm{TL} = -0.1\mathrm{PC}^3 + 3.9\mathrm{PC}^2 + \mathrm{PC} - 3.4\log(L) + 11.0 \tag{23}$$

where a logaritmic fit plus a constant was used for parameter D in table 2. The new regression curves for the low-frequency range found in equation (23) can be seen in figure 5. The coefficients of determination R^2 found with the proposed regressions curve in equation (23) are given in table 3. There is only a slight decrease from the regression curves in table 2 where the parameters A, B and C were determined separately with the data per junction length.

Table 3: Coefficients of determination R^2 for proposed regression curve in equation (23)

Junction length	2 m	3 m	4 m	5 m	6 m	7 m	8 m
Coefficients of determination R^2	0.962	0.975	0.974	0.973	0.972	0.971	0.970

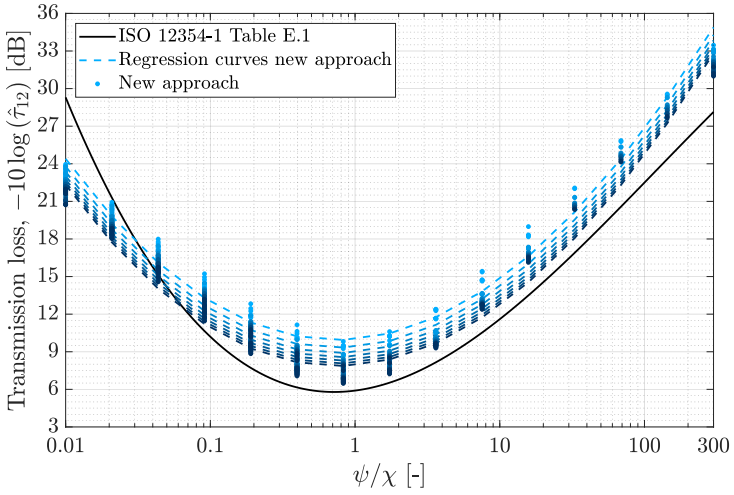

Figure 5: Results using the new approach in low-frequency range (50-200 Hz) together with the new regression curves found in equation (23) and with the regression curve from ISO 12354-1. Lightblue dots correspond to a junction length of 2 m and darkblue to a junction length of 8 m. The colors used for plotting results of intermediate junction lengths are interpolated between light- and darkblue.

The transmission losses found in the mid-frequency range with the new approach are shown in figure 6, together with the regression curves from ISO 12354-1 [6]. Like in the low frequency range, it can be seen that the new approach results in a prediction for the transmission loss that is higher than the regression curve from the international standard. Also the finite element simulations in the work of Hopkins et al. [7] resulted in higher transmission losses than the regression curve.

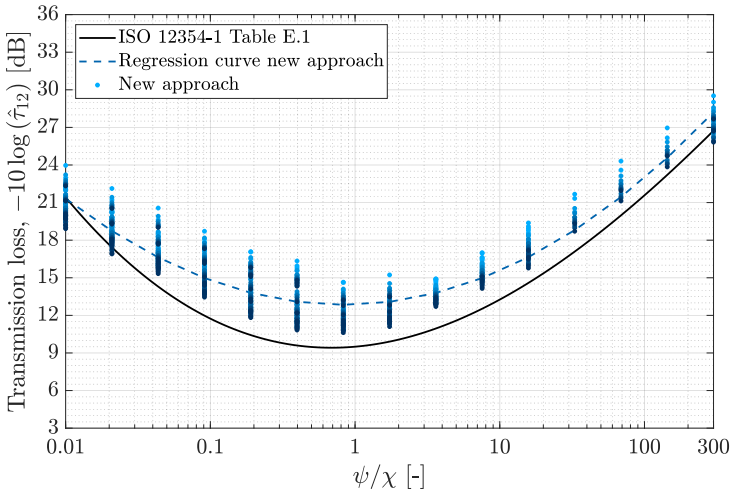

Figure 6: Results using the new approach in mid-frequency range (200-1000 Hz) together with the regression curve from ISO 12354-1. Lightblue dots correspond to a junction length of 2 m and darkblue to a junction length of 8 m. The colors used for plotting results of intermediate junction lengths are interpolated between light- and darkblue.

Figure 6 shows no clear relation between junction length and transmission loss and the results are spread further apart than in the low-frequency range, indicating that the ratio of characteristic moment impedances might not be the optimal choice as the independent variable when plotting results in this frequency range. The ratio of characteristic moment impedances is based on the surface mass and bending stiffness of the connected plates (see equation (21)). In the low-frequency range transmission of bending waves dominates the vibration transmission between the two plates but in the

mid-frequency range in-plane and shear waves also have an influence, which explains why the ratio of characteristic moment impedances might not be the best choice as an independent variable in this frequency range. Due to the spread on the results seen in figure 6, for now a single regression curve is proposed for the mid-frequency range, also shown in figure 6.

$$\mathrm{TL} = -0.01\mathrm{PC}^3 + 2.3\mathrm{PC}^2 + 0.4\mathrm{PC} + 12.9 \tag{24}$$

The coefficient of determination R^2 for the regression curve in equation (24) equals 0.902.

The transmission losses found in the high-frequency range with the new approach are shown in figure 7, together with the regression curves from ISO 12354-1 [6]. In the high frequency range, the results are spread further apart than in the mid-frequency range, indicating that also in the high-frequency range there is a need for another independent variable instead of the ratio of characteristic moment impedances, due to the importance of in-plane waves in the high-frequency range.

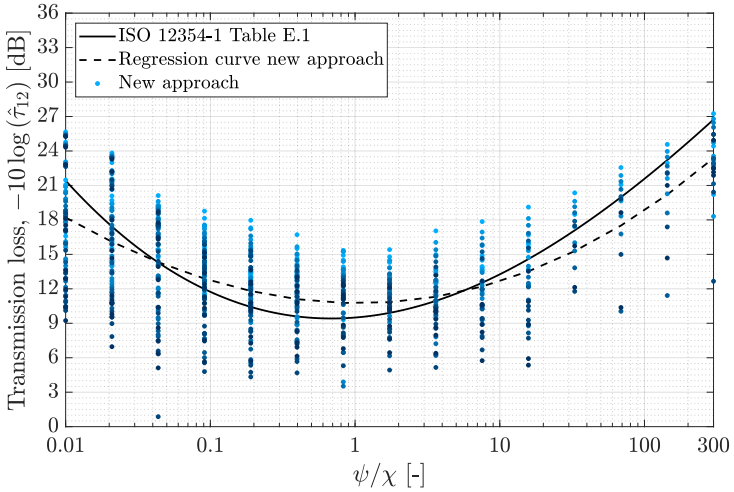

Figure 7: Results using the new approach in high-frequency range (1250-3150 Hz) together with the regression curve from ISO 12354-1. Lightblue dots correspond to a junction length of 2 m and darkblue to a junction length of 8 m. The colors used for plotting results of intermediate junction lengths are interpolated between light- and darkblue.

Similarly to the mid-frequency range, a single regression curve is proposed, which is also plotted in figure 7.

$$\mathrm{TL} = -0.06\mathrm{PC}^3 + 1.9\mathrm{PC}^2 - 0.1\mathrm{PC} + 10.7 \tag{25}$$

The coefficient of determination R^2 for the regression curve in equation (25) equals 0.428, clearly indicating the need for a different independent variable.

4. CONCLUSIONS

A new approach for calculating vibration transmission across junctions based on diffuse field reciprocity has been presented. In contrary to the conventional approach, where the transmission coefficient is calculated for multiple incident wave angles and then integrated to calculate the mean diffuse field transmission coefficient, the new approach calculates the transmission coefficient using the coupling loss factor. The coupling loss factor is calculated based on the direct field dynamic stiffness matrices of the plates connected to the junction. The direct field dynamic stiffness matrix

of a plate can be determined in multiple ways. Two possible methods were considered in this work, where the first uses thin plate theory to analytically derive the direct field dynamic stiffness matrix of a thin, isotropic, semi-infinite plate in the wavenumber domain. Since the assumption of thin plates is only valid at low frequencies, a second method is considered which uses a combination of 2.5D finite elements and perfectly matched layers to calculate the direct field dynamic stiffness matrix in the wavenumber domain. To transform this result from the wavenumber domain to the spatial domain a correction for the finite junction length is applied.

As a case study, the method is applied to an L-junction consisting of two perpendicular plates. For all considered ranges, results found using the new approach are generally higher than the regression curve found in the international standard. This is due to the wave theory results used for the regression curves in combination with results obtained using finite elements. Wave theory assumes an infinite junction, resulting in lower transmission losses.

In the low-frequency range a clear relation can be found between transmission loss and the length of the junction. Cubic regression curves are determined for the data per junction length and good fits are found found with the cubic curves. A single regression curve is proposed which depends on the junction length. With this single regression curve there is only a slight decrease in the coefficient of determination.

In the mid-frequency range, a larger spread of the predicted transmission losses could be observed and no clear relation between junction length and transmission loss could be seen. In this frequency range the ratio of characteristic moment impedances might not be the best choice as the independent variable when plotting results. The ratio of characteristic moment impedances is based on the surface mass and bending stiffness of the connected plates. In the low-frequency range transmission of bending waves dominates the vibration transmission between the two plates but in the mid-frequency range in-plane waves also have an influence. Due to the spread of the transmission losses, for now a single regression curve is proposed.

Finally, in the high-frequency range the results are spread further apart than in the mid-frequency range, indicating that also in the high-frequency range there is a need for another independent variable. In the high-frequency range, like in the mid-frequency range, for now a single regression curve is proposed. Further research could results in finding a better independent variable for plotting results in the mid- and high-frequency range which should also take into account the effect of the in-plane and shear waves in the mid- and high-frequency range.

ACKNOWLEDGEMENTS

The research presented in this paper has been performed within the frame of the VirBAcous project (project ID 714591) “Virtual building acoustics: a robust and efficient analysis and optimization framework for noise transmission reduction” funded by the European Research Council in the form of an ERC Starting Grant. The financial support is gratefully acknowledged.

REFERENCES

[1] C. Hopkins. *Sound insulation*. Elsevier Ltd., Oxford, 2007.

[2] R.J.M. Craik. *Sound transmission through buildings using statistical energy analysis*. Gower, Aldershot, UK, 1996.

[3] L. Cremer and M. Heckl. *Structure-borne sound: Structural vibrations and sound radiation at audio frequencies*. Springer, Berlin, 2nd edition, 1988.

[4] R. S. Langley and K. H. Heron. Elastic wave transmission through plate/beam junctions. *Journal of Sound and Vibration*, 143(2):241–253, 1990.

[5] P.J. Shorter and R.S. Langley. Vibro-acoustic analysis of complex systems. *Journal of Sound and Vibration*, 288(3):669–699, 2005.

[6] International Organization for Standardization. *ISO 12354-1:2017: Building Acoustics - Estimation of acoustic performance of buildings from the performance of elements - Part 1: Airborne sound insulation between rooms*, 2017.

[7] C. Hopkins, C. Crispin, J. Poblet-Puig, and C. Guigou-Carter. Regression curves for vibration transmission across junctions of heavyweight walls and floors based on finite element methods and wave theory. *Applied Acoustics*, 113:7–21, 2016.

[8] R. S. Langley. A derivation of the coupling loss factors used in statistical energy analysis. *Journal of Sound and Vibration*, 141(2):207–219, 1990.

[9] S. François, M. Schevenels, G. Lombaert, P. Galvín, and G. Degrande. A 2.5D coupled FE-BE methodology for the dynamic interaction between longitudinally invariant structures and a layered halfspace. 199(23-24):1536–1548, 2010.

[10] U. Basu and A.K. Chopra. Perfectly matched layers for time-harmonic elastodynamics of unbounded domains: theory and finite-element implementation. *Computer Methods in Applied Mechanics and Engineering*, 192(11-12):1337–1375, 2003.

[11] V. Cotoni, P. Shorter, and R. Langley. Numerical and experimental validation of a hybrid finite element-statistical energy analysis method. *Journal of the Acoustical Society of America*, 122(1):259–270, 2007.